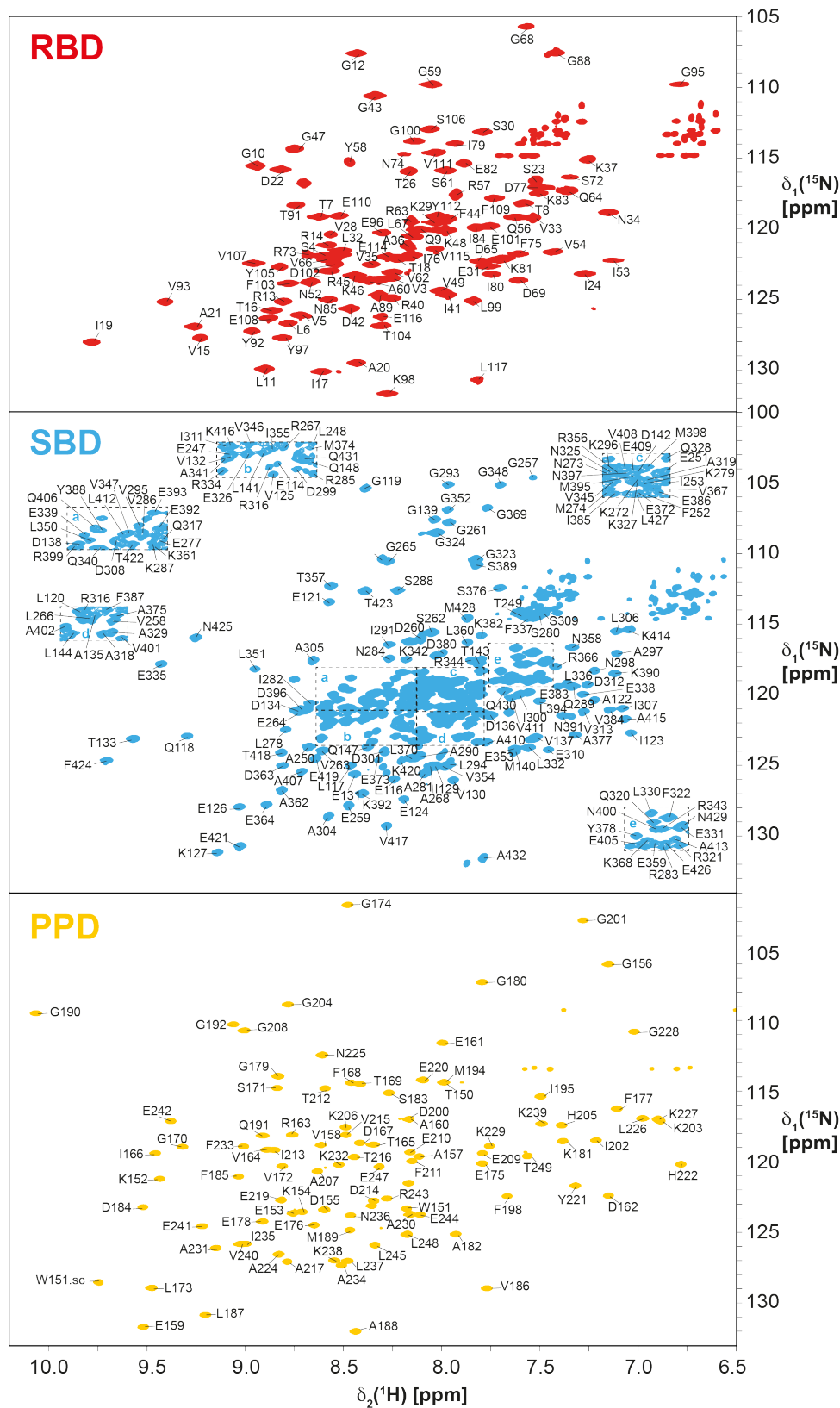
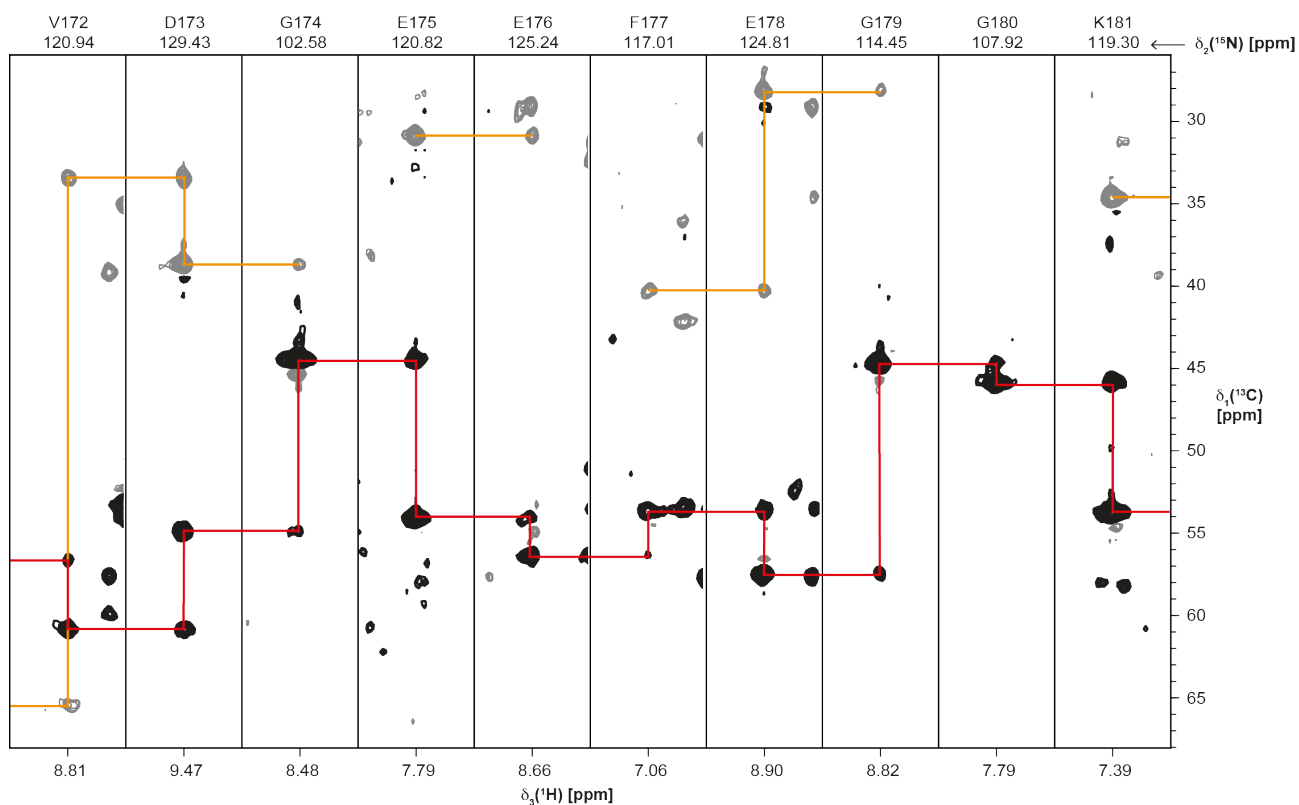


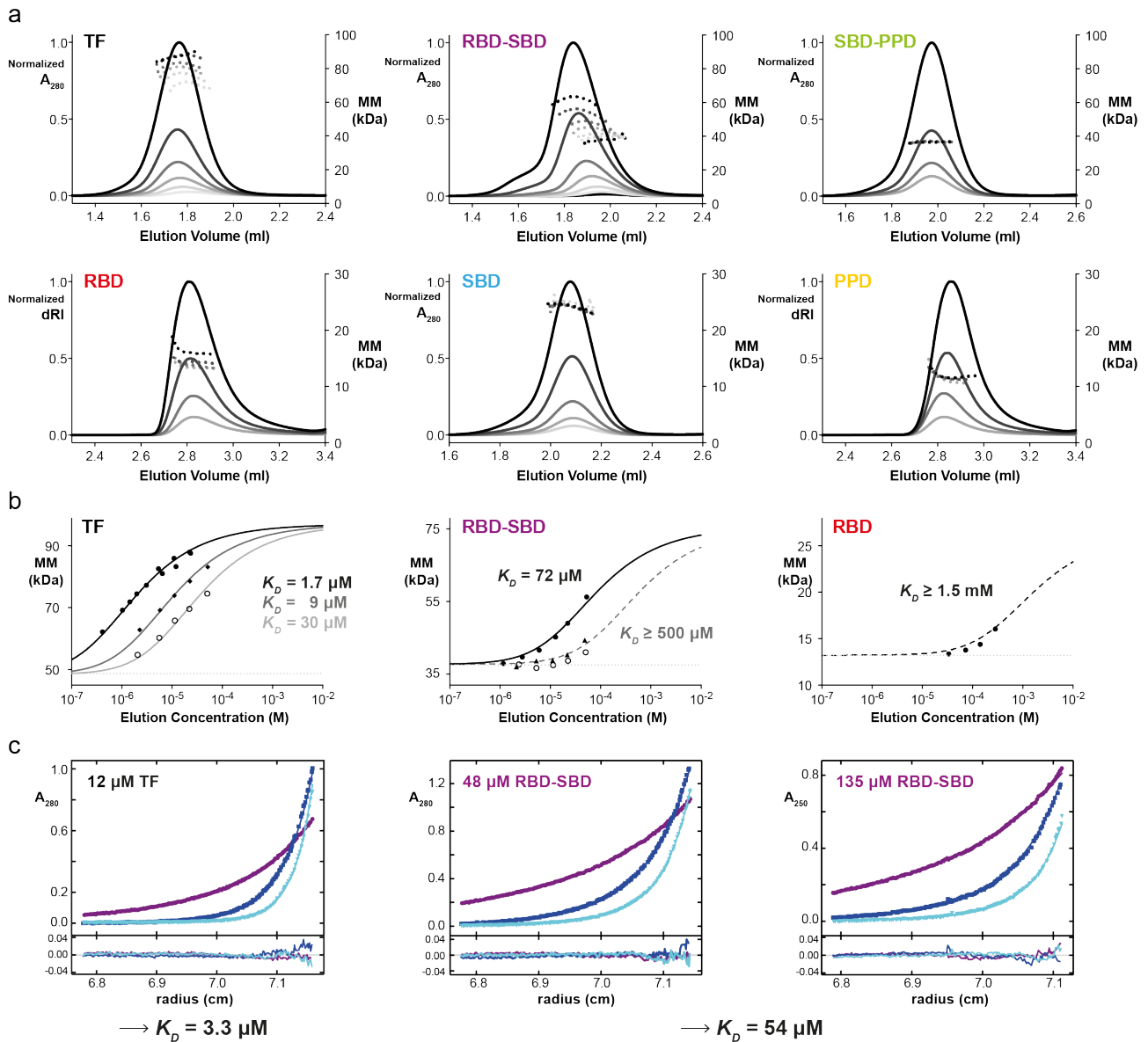
Supplementary Figures



Supplementary Figure 1 | Sequence-specific resonance assignment of TF domain constructs. 2D [^{15}N , ^1H]-TROSY spectrum of 100 μM [$U\text{-}^{15}\text{N}$] RBD, 250 μM [$U\text{-}^2\text{H}$, ^{15}N] SBD, and 100 μM [$U\text{-}^{15}\text{N}$] PPD in sample buffer (20 mM K-phosphate pH 6.5, 100 mM KCl, 0.5 mM EDTA) at 25 $^\circ\text{C}$ and 700 MHz. The sequence-specific resonance assignments were obtained from 3D triple resonance experiments, and confirmed by comparison with published data (BMRB 15813¹ and BMRB 19835–19837²).

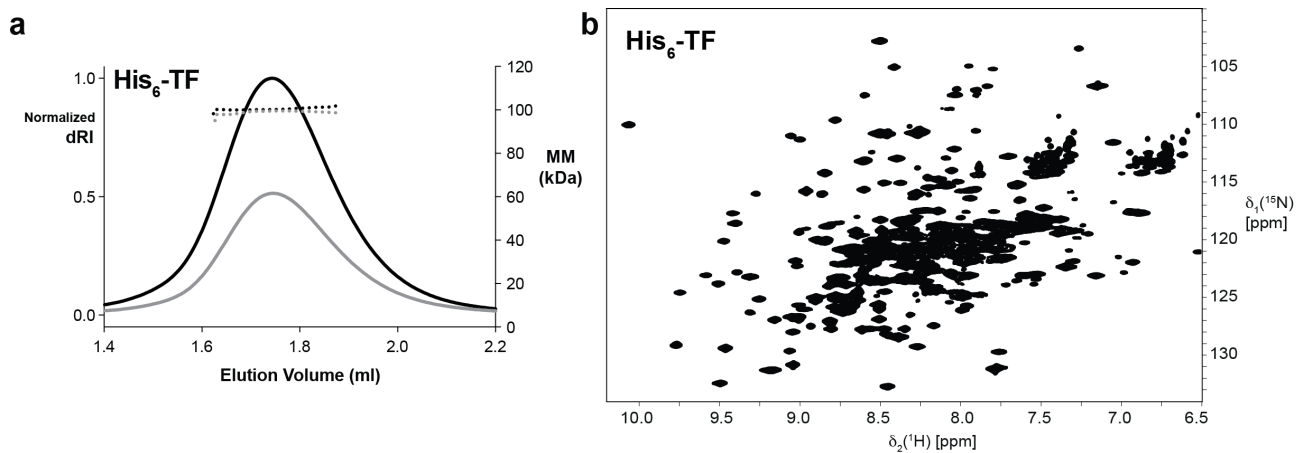


Supplementary Figure 2 | Backbone NMR assignment of SBD-PPD. Strips for residues 172–181 from a 3D TROSY-HNCACB experiment for $[U\text{-}^2\text{H}, ^{15}\text{N}, ^{13}\text{C}]$ SBD-PPD acquired in sample buffer (20 mM K-phosphate pH 6.5, 100 mM KCl, 0.5 mM EDTA) at 25 °C and 700 MHz. The red and orange lines indicate the sequential connection between the strips for $^{13}\text{C}\alpha$ and $^{13}\text{C}\beta$ nuclei, respectively.

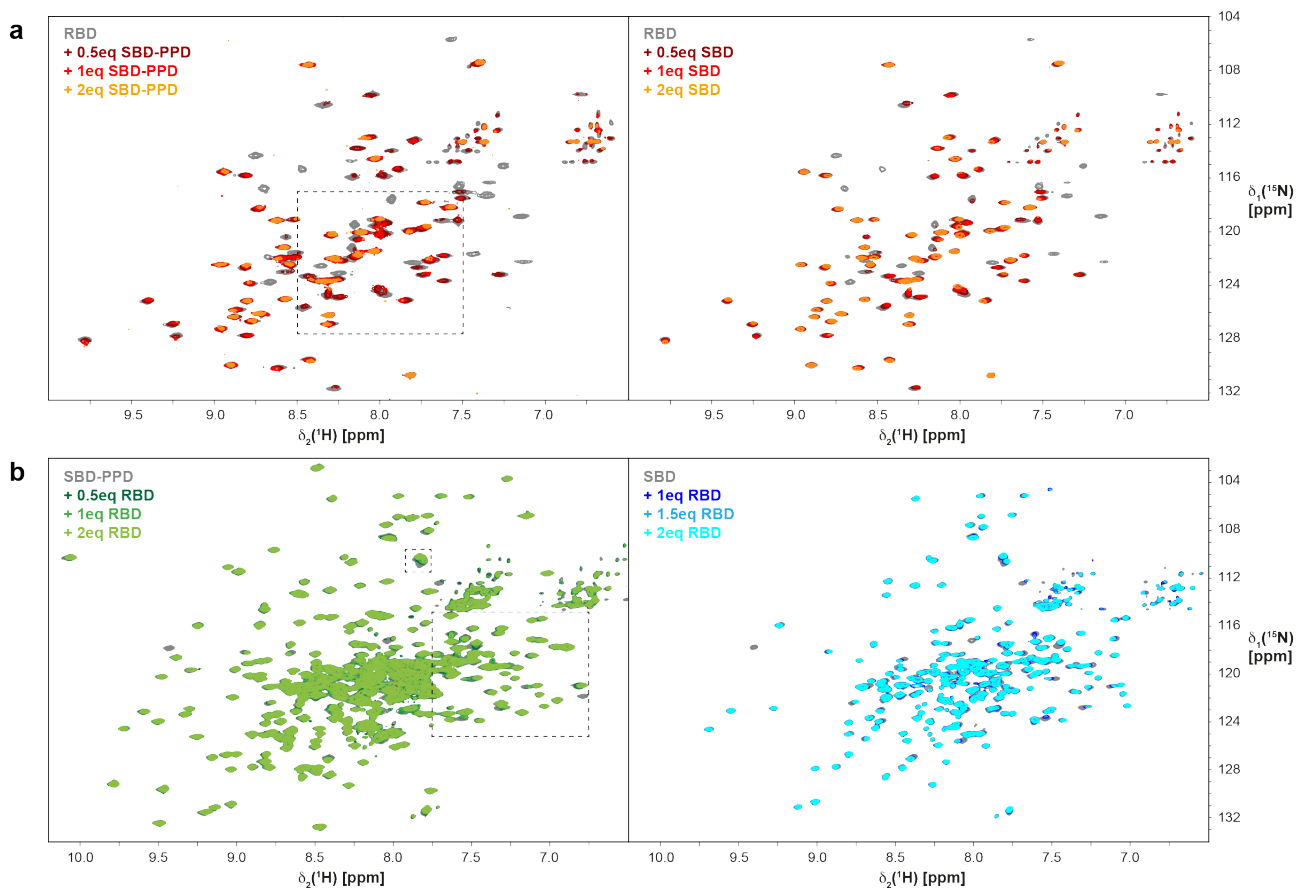


Supplementary Figure 3 | Biophysical characterization of TF domain construct dimerizations.

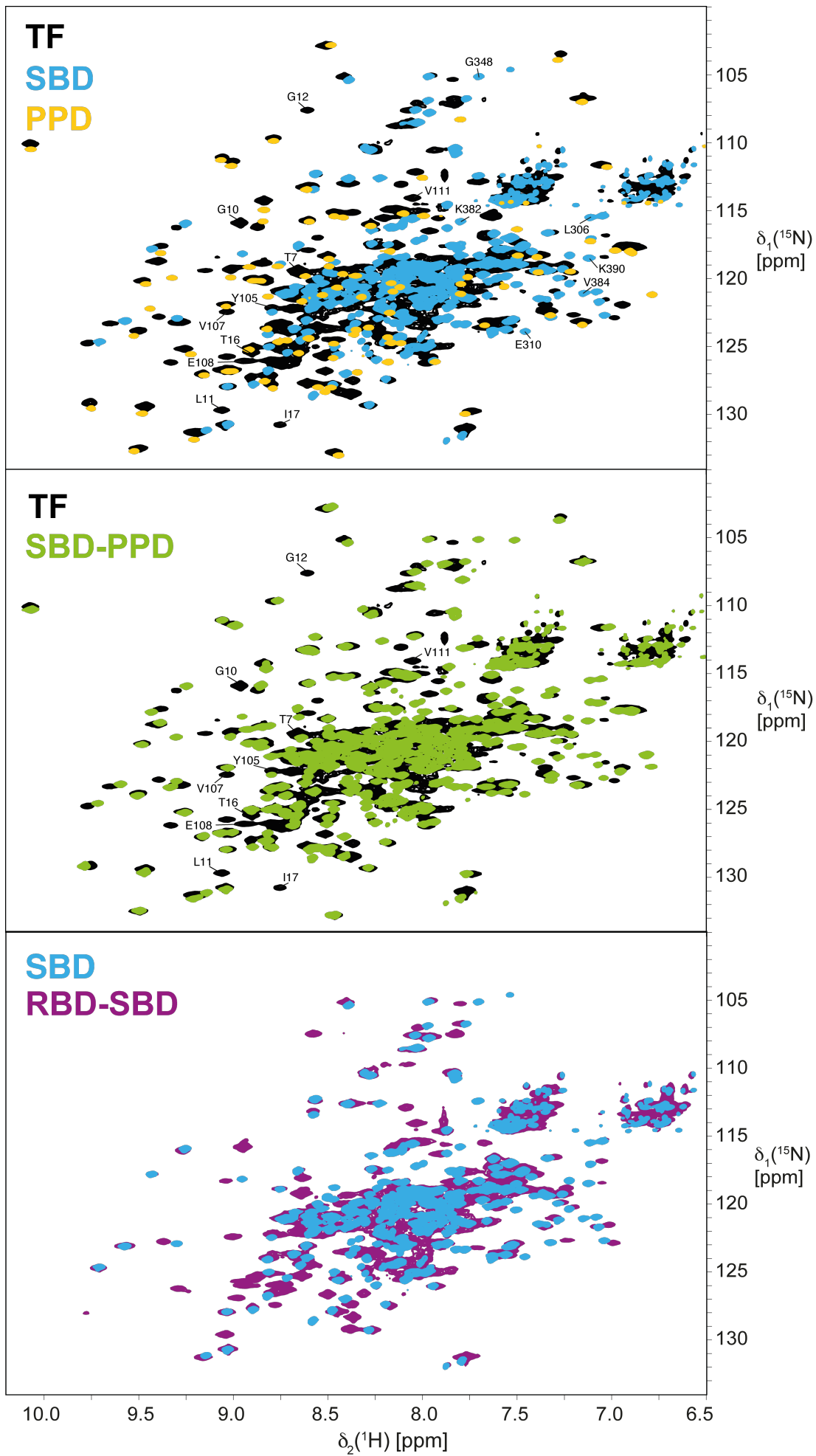
Measurements were performed in sample buffer at 6 °C. **(a)** SEC elution profiles plotted as normalized absorbance (A_{280}) or normalized differential refractive index (dRI) (solid lines, left axis) and MALS apparent molecular mass (dotted lines, right axis) as a function of protein concentrations of the indicated domain constructs. **(b)** Nonlinear regression fit of the averaged molar mass as a function of the elution concentration to a monomer-dimer equilibrium³. For TF and RBD–SBD fittings are plotted for three different salt concentrations: 100 mM KCl (closed circles and black line), 250 mM KCl (closed diamonds and dark gray line) and 500 mM KCl (open circles and light gray line). **(c)** Analytical ultracentrifugation (AUC) profiles for 12 μM TF as well as 48 μM and 135 μM RBD–SBD. Data are shown for three centrifugation speeds (10, 16, and 20 krpm, in purple, blue, and cyan, respectively). For each construct, all data were globally fitted to a single monomer-dimer equilibrium. Residuals are shown below.

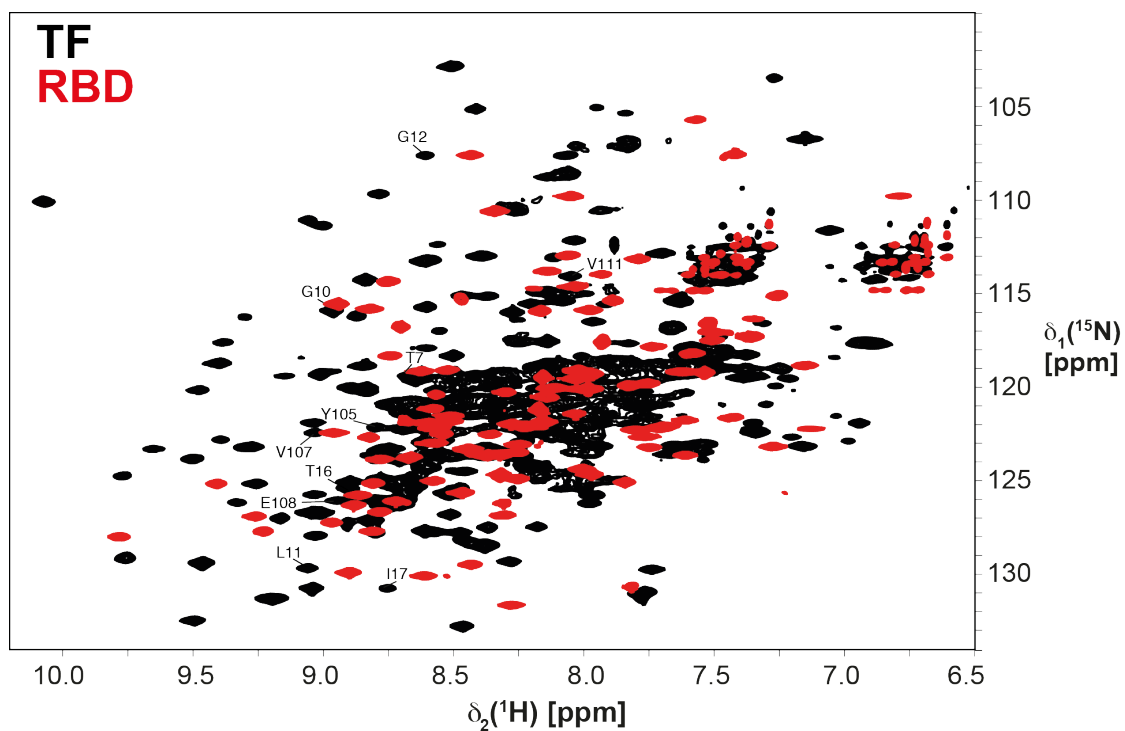


Supplementary Figure 4 | Characterization of His₆-TF. (a) SEC elution profile plotted as normalized differential refractive index (dRI) and MALS apparent molecular mass (dotted lines, right axis) as a function of protein concentrations. Elution concentration is 20 μ M and 10 μ M for black and gray lines, respectively, showing that the dimer dissociation constant K_D must be below 100 nM. (b) 2D [¹⁵N, ¹H]-TROSY spectrum of 300 μ M [*U*-²H, ¹⁵N] His₆-TF in sample buffer (20 mM K-phosphate pH 6.5, 100 mM KCl, 0.5 mM EDTA) at 25 °C and 700 MHz.



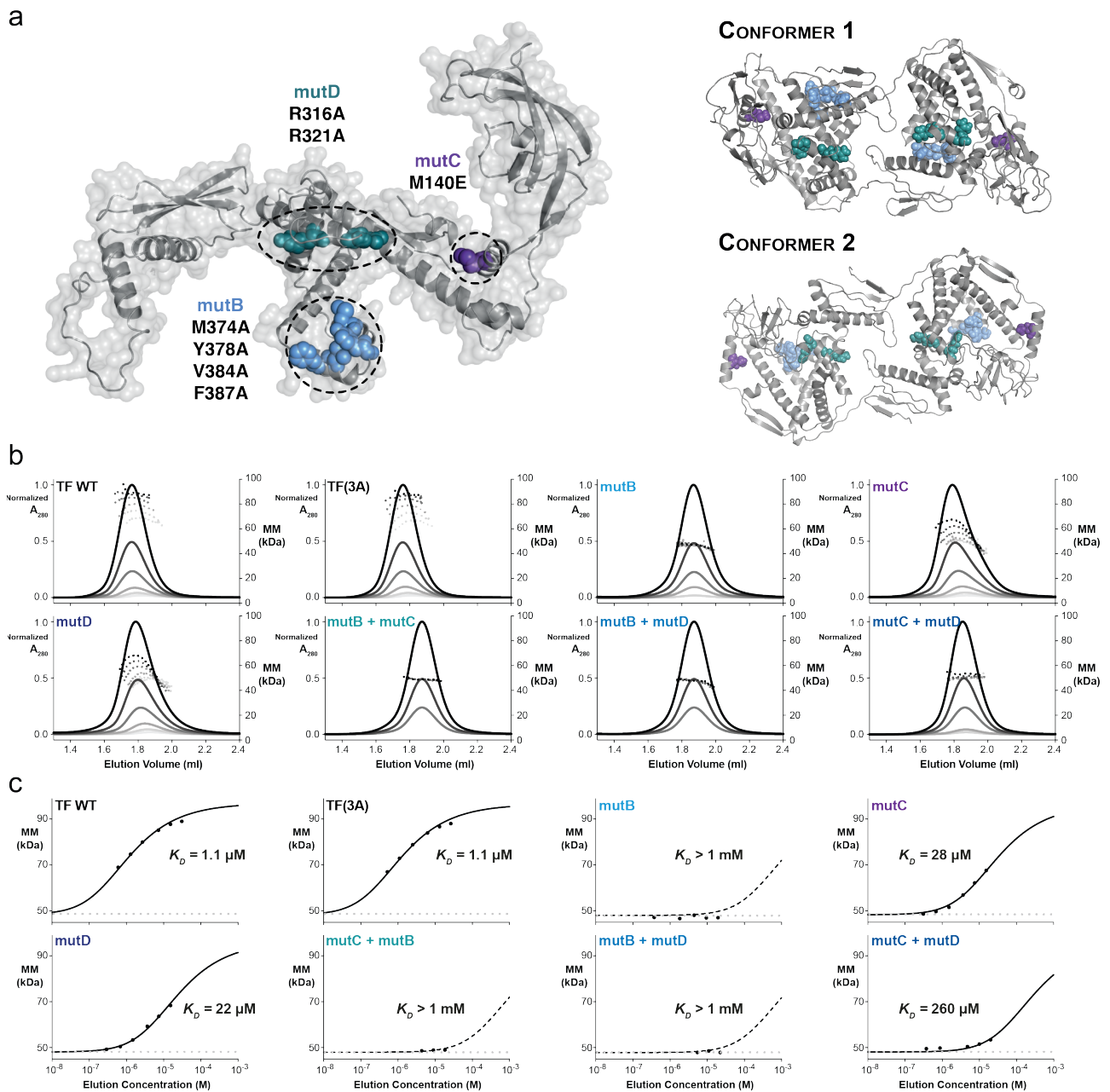
Supplementary Figure 5 | NMR titrations of monomeric TF domains. (a) Titration of unlabeled SBD–PPD to 100 μM [$U\text{-}^{15}\text{N}$] RBD (left) and of unlabeled SBD to 100 μM [$U\text{-}^{15}\text{N}$] RBD (right). **(b)** Titration of unlabeled RBD to 250 μM [$U\text{-}^2\text{H}, ^{15}\text{N}$] SBD–PPD and of unlabeled RBD to 100 μM [$U\text{-}^2\text{H}, ^{15}\text{N}$] SBD. The dashed rectangles correspond to the zoomed regions in Figure 3. Spectra were acquired in sample buffer (20 mM K-phosphate pH 6.5, 100 mM KCl, 0.5 mM EDTA) at 25 $^\circ\text{C}$ and 700 MHz.



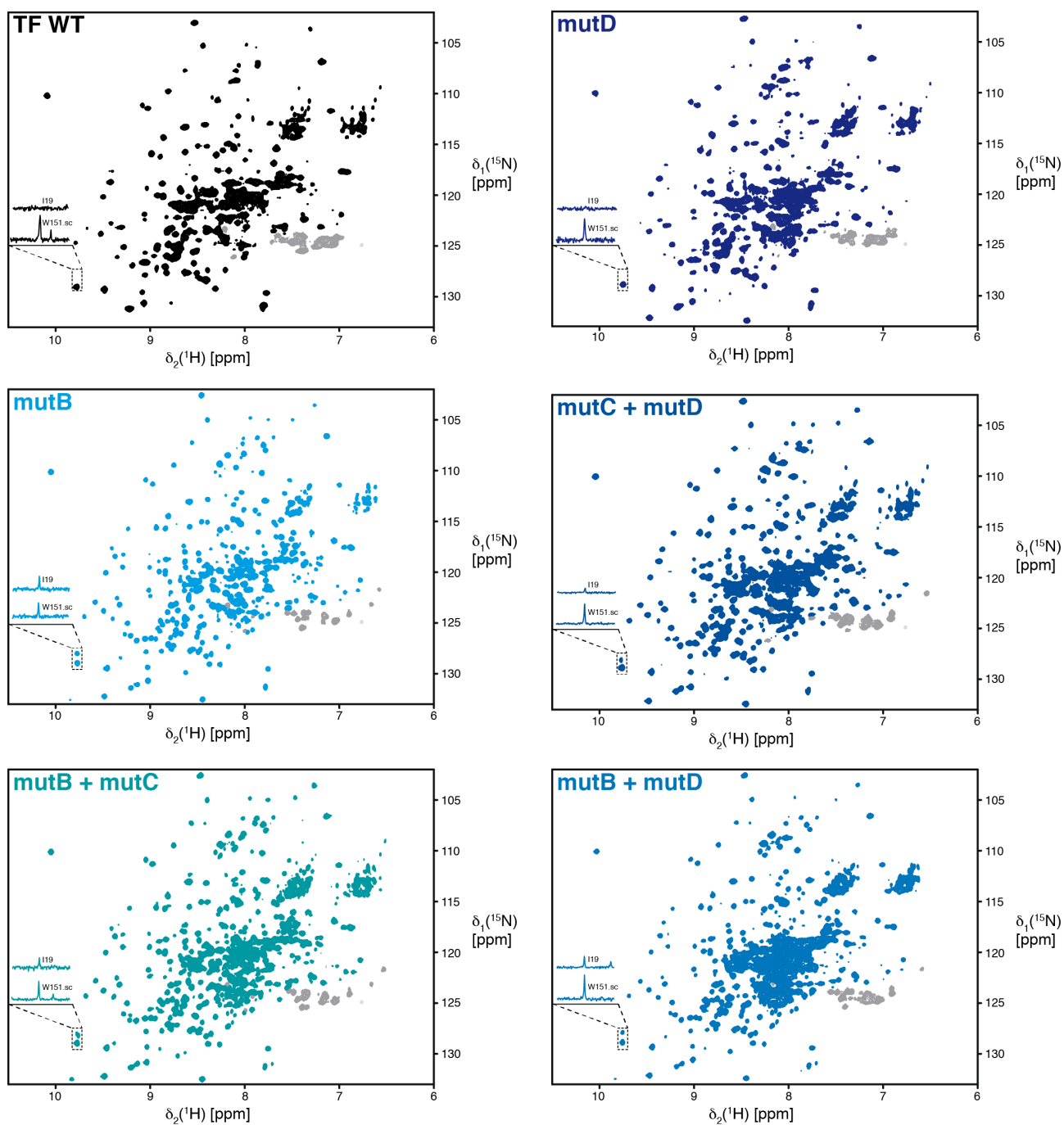


Supplementary Figure 6 | NMR resonances of the RBD are line-broadened in full-length TF and RBD–SBD.

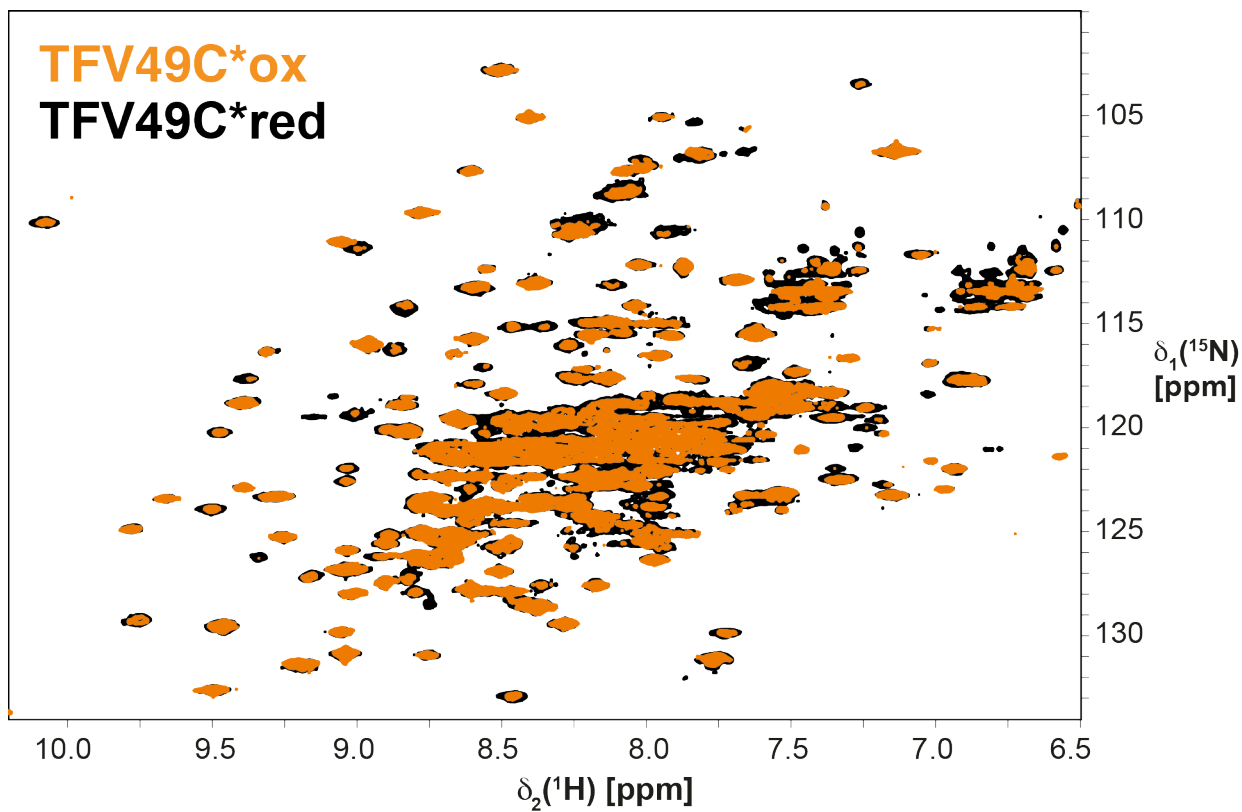
Overlays of 2D $[^{15}\text{N},^1\text{H}]$ -TROSY spectra of 500 μM $[U\text{-}^2\text{H},^{15}\text{N}]$ TF (black), $[U\text{-}^2\text{H},^{15}\text{N}]$ SBD (blue), $[U\text{-}^{15}\text{N}]$ PPD (yellow), $[U\text{-}^2\text{H},^{15}\text{N}]$ SBD–PPD (purple), $[U\text{-}^2\text{H},^{15}\text{N}]$ RBD (red), and 250 μM $[U\text{-}^2\text{H},^{15}\text{N}]$ SBD–PPD (green). The spectra were acquired in sample buffer (20 mM K-phosphate pH 6.5, 100 mM KCl, 0.5 mM EDTA) at 25 °C and 700 MHz. Only 16 out of 108 expected RBD resonances are observed in full-length TF. Ten of these 16 resonances could be unambiguously assigned by comparison with the spectrum of the isolated RBD, together with the 3D TROSY HNCACB for $[U\text{-}^2\text{H},^{15}\text{N},^{13}\text{C}]$ -TF. Several resonances of the SBD are line-broadened in TF full length, but not in the isolated SBD. The assignment of five of these resonances are indicated in the overlay of SBD / TF.



Supplementary Figure 7 | Validation of the TF dimer structure by mutagenesis. (a) Location of the mutation sets mutB, mutC, and mutD on the TF crystal structure (PDB 1W26) and conformers 1 and 2 of the TF dimer. (b) Biophysical characterization of TF mutants. Measurements were performed in sample buffer at 26°C. SEC elution profiles plotted as normalized absorbance (A_{280}) (solid lines, left axis) and MALS apparent molecular mass (dotted lines, right axis) as a function of protein concentrations of the indicated mutants. (c) Nonlinear regression fit of the averaged molar mass as a function of the elution concentration to a monomer-dimer equilibrium.



Supplementary Figure 8 | Mutations at the dimer interface lower TF dimerization K_D . 2D [^{15}N , ^1H]-TROSY spectrum of 200 μM [U - ^2H , ^{15}N] TF and mutants acquired in sample buffer (20 mM K-phosphate pH 6.5, 100 mM KCl, 0.5 mM EDTA) at 25 $^\circ\text{C}$ and 700 MHz. In each spectrum a 1D-trace corresponding to W151 side-chain and to I19 is shown. The mutations lower the affinity between the protomers and peaks corresponding to residues that belong to the RBD become visible in the spectra.



Supplementary Figure 9 | Measurement of paramagnetic relaxation enhancement. Overlay of 2D [^{15}N , ^1H]-TROSY spectra of 300 μM [$U\text{-}^2\text{H}$, ^{15}N] TF(V49C), spin labeled with MTSL in the paramagnetic oxidized state (orange) and the diamagnetic reduced state (black). Spectra were recorded in sample buffer (20 mM K-phosphate pH 6.5, 100 mM KCl, 0.5 mM EDTA) at 25 $^\circ\text{C}$ and 700 MHz.

Supplementary Tables

Supplementary Table 1 | Interaction matrix of TF domain constructs^a:

	RBD	SBD	PPD	SBD-PPD	RBD-SBD	TF
RBD	-	+	-	+	n.d.	n.d.
SBD	+	-	-	-	n.d.	n.d.
PPD	-	-	-	-	n.d.	n.d.
SBD-PPD	+	-	-	-	n.d.	n.d.
RBD-SBD	n.d.	n.d.	n.d.	n.d.	+	n.d.
TF	n.d.	n.d.	n.d.	n.d.	n.d.	+

^aDiagonal entries were determined by SEC-MALS and AUC (Table 1) and off-diagonal entries by NMR spectroscopy. (+) = detectable interaction; (-) = no interaction detected; n.d. = not determined

Supplementary Table 2 | Input parameters for HADDOCK docking and output parameters for the two structural clusters with highest ranks.

HADDOCK input parameters		
<i>Number of active residues^a</i>		
Molecule A ^b		38
Molecule B ^c		64
<i>Symmetry restraints</i>		432
HADDOCK output		
	<i>Cluster 1</i>	<i>Cluster 2</i>
HADDOCK score	-153.7 ± 12.3	-118.2 ± 16.4
Cluster size	9	22
Average pairwise backbone RMSD within the cluster	0.94 ± 0.34	0.47 ± 0.12
Backbone RMSD between the lowest-energy structures	15.8	

^a residues for which significant line-broadening or significant chemical shift perturbation was observed upon interaction

^b active residues on RBD

^c active residues on SBD

Supplementary Table 3 | Input data for structure refinement with XPLOR-NIH.

Constraint type	Amount	
<i>EFN restraint</i>	3116/monomer	
<i>PRE restraint</i>	<i>Intra- or intermolecular A-A, B-B or A-B, B-A (medium distance)</i>	<i>Intra- and intermolecular A-A, B-B, A-B, B-A (long distance)</i>
S30C	6	95
V49C	63	32
S61C	51	32
S72C	10	75
A223C	27	45
E326C	14	71
Total	171	350

Supplementary Table 4 | XPLOr-NIH structural statistics.

XPLOr-NIH output	<i>Conformer 1</i>	<i>Conformer 2</i>
<i>Structure statistics</i> ^a		
Intramolecular restraints	42	44
Intermolecular restraints	129	127
<i>Violations long-distance PRE restraints</i> ^a		
Number of violations (>0.5 Å)		
Intramolecular	1	0
Intermolecular	4	1
Average violations (Å)		
Intramolecular	2.64	-
Intermolecular	1.42 ± 0.75	0.57
Max. PRE distance constraint violation (Å)		
Intramolecular	2.64	-
Intermolecular	2.47	0.57
<i>Violations medium-distance PRE restraints</i> ^a		
Number of violations (>0.5 Å)		
Intramolecular	14	16
Intermolecular	33	29
Average violations (Å)		
Intramolecular	1.52 ± 0.97	1.80 ± 1.03
Intermolecular	1.90 ± 1.25	1.63 ± 1.01
Max. PRE distance constraint violation (Å)		
Intramolecular	3.21	4.43
Intermolecular	5.17	4.97
<i>Deviations from idealized geometry</i> ^a		
Bond lengths (Å)	0.005	0.005
Bond angles (°)	0.539	0.572
Impropers (°)	0.841	0.965
<i>Ramachandran analysis</i> ^b		
Most favored regions (%)	90.8	86.6
Additional allowed regions (%)	7.6	9.9
Generously allowed regions (%)	1.0	1.6
Disallowed regions (%)	0.5	1.9
<i>Average pairwise rmsd (Å)</i> ^c		
Heavy atoms	2.13 ± 0.73	1.74 ± 0.79
Backbone atoms	2.04 ± 0.74	1.66 ± 0.79

^a Calculated for the lowest energy structures

^b Calculated with PROCHECK-NMR for the ensemble of the 10 lowest energy structures

^c Pairwise rmsd calculated with PyMOL between the 10 lowest energy structures

Supplementary Table 5 | Dimer dissociation constants of TF mutants.

Mutant sets ^a	K_D (μM)
–	1.1 ± 0.2
mutB	> 1000
mutC	28 ± 4
mutD	22 ± 3
mutD + mutC	260 ± 130
mutB + mutC	> 1000
mutB + mutD	> 1000

^a introduced on the TF(3A) background

Supplementary Table 6 | Primer sequences used for cloning.

Primer	Sequence
TF_fw	GGAATTCCATATGCAAGTTTCAGTTGAAACC
TF_rev	ACACGCGGCCGCTTACGCCTCTGGTTCATCAGC
TF_117_Stop_fw	CCGGAAGTTGAACTGTAGGGTCTGGAAGCGA
TF_117_Stop_rev	TCGCTTCCAGACCCTACAGTTCAACTTCCGG
TF_RF_114fw	GGTGCCGCGCGGCAGCCATATGGAAGTTGAACTGCAGGGTCT
TF_RF_432rev	GGTGCTCGAGTGCGGCCGCTTACGCCTGCTGGTTCATCAG
TF_RF_fw	GTGCCGCGCGGCAGCCATATGCAAGTTTCAGTTGAAACCAC
TF_RF_149rev	GGTGGTGGTGGTGGTGTCTCGAGCTGCTGTTTACGCAGAGTATCC
TF_RF_149/249_fw	CGGCATGCTGGATACTCTGCGTAAACAGCAGGAACTGACTGCAGAATTCATCAA
TF_RF_149fw	GGTGCCGCGCGGCAGCCATATGGCGACCTGGAAGAAAAAGAC
TF_RF_249rev	GGTGCTCGAGTGCGGCCGCTTAAGTCAGTTCCGGCAGTTC
Thr2TEV_fw	GCCATCATCATCATCACAGCGAGAACCTATATTTCCAGGGCAGCCATATG
Thr2TEV_rev	CATATGGCTGCCCTGGAAATATAGGTTCTCGCTGTGATGATGATGATGATGGC
TF_S30C_fw	GACCAGCTCGCATTTAACAGCGGTCTCGATGCT
TF_S30C_rev	GACCAGCTCGCATTTAACAGCGGTCTCGATGCT
TF_V49C_fw	TTGACGGCTCCGCAAAGGCAAATGCCCAATGAATATCGTTGCTC
TF_V49C_rev	GAGCAACGATATTCATTGGGCATTTGCCTTTGCGGAAGCCGTCAA
TF_S61C_fw	GCGTTATGGCGCGTGTGTACGCCAGG
TF_S61C_rev	CCTGGCGTACACACGCGCCATAACGC
TF_S72C_fw	TTCTGGGTGACCTGATGTGCCGTAACCTTCATTGAC
TF_S72C_rev	GTCAATGAAGTTACGGCACATCAGGTCACCCAGAA
TF_A223C_fw	ACCTTCCCGGAAGAATACCACTGCGAAAACCTGAAAGGTAAAGCA
TF_A223C_rev	TGCTTACCTTTCAGGTTTTTCGAGTGGTATTCTTCCGGGAAGGT
TF_E326C_fw	CACAGCGTTTCGGTGGCAACTGCAAACAAGCTCTGGAAGTCC
TF_E326C_rev	GGCAGTTCAGAGCTTGTTCAGTTGCCACCGAAACGCTGTG
TF_FRK44-46_AAA_fw	GTTGCGAAAAAAGTACGTATTGACGGCGCCGCCGAGGCAAAGTGCCAATGAATATCGTTGC
TF_FRK44-46_AAA_rev	GCAACGATATTCATTGGCACTTTGCCTGCGGCGGCCGCTCAATACGTACTTTTTTCGCAAC
TF_R321A_fw	GCCAGGCTGCACAGGCTTTCGGTGGCAACG
TF_R321A_rev	CGTTGCCACCGAAAGCCTGTGCAGCCTGGC
TF_R316A_fw	GCGAAATCGACGTTTCTGCGTGCCAGGCTGCAC
TF_R316A_rev	GTGCAGCCTGGGCACGCAGAACGTCGATTTTCGC
TF_M140E_fw	GCTGACGTTGACGGCGAGCTGGATACTCTGCG
TF_M140E_rev	CGCAGAGTATCCAGCTCGCCGTCAACGTCAGC
TF_V384A_F387A_fw	GCGTACGAAGATCCGAAAGAAGCTATCGAGGCCTACAGCAAAAACAAAGAAGT
TF_V384A_F387A_rev	CAGTTCTTTGTTTTGCTGTAGGCCTCGATAGCTTCTTTCCGGATCTTCGTACGC
TF_M374A_Y378A_fw	AAGGCCTGATCGAAGAGCGGCTTCTGCGGCCGAAGATCCGAAAGAAG
TF_M374A_Y378A_rev	CTTCTTTCGGATCTTCGGCCGAGAAGCCGCTCTTCGATCAGGCCTT

Supplementary Notes

Supplementary Note 1

Kinetic equations for the determination of the lifetime of the TF dimer

The monomer-dimer equilibrium for the two differently labeled forms of TF is described by the following chemical equilibrium reactions



where N and S are the ^{15}N -labeled and spin-labeled forms of monomeric TF, respectively. The three reactions 1–3 have the same k_{off} , k_{on} and K_d values. The experimental conditions were chosen to have equal amounts of the two labeled forms:

$$[N]_{\text{total}} = [S]_{\text{total}} \quad (4)$$

At $t = 0$, equal samples of pure N and pure S are mixed and the equations hold:

$$[N_2]_0 = [S_2]_0 = c \quad \text{and} \quad [NS]_0 = 0 \quad (5)$$

The symmetry argument (K_d is the same for N_2 , S_2 , and NS) yields that at all times

$$[N_2] = [S_2] \quad (6)$$

Furthermore, symmetry considerations yield that at all times

$$[N] = [S] = \text{const} \quad (7)$$

and

$$[N_2] + [NS] + [S_2] = 2c \quad , \text{ rewritten as} \quad [NS] = 2c - 2[N_2] \quad (8)$$

After mixing of the samples, the system evolves from

$$[N_2]_0 = [S_2]_0 = c \quad \text{and} \quad [NS]_0 = 0 \quad \text{at} \quad t = 0 \quad (5)$$

to

$$[N_2]_{\text{eq}} = [S_2]_{\text{eq}} = [NS]_{\text{eq}} = \frac{2}{3}c \quad \text{at} \quad t = \infty \quad (9)$$

The rate equations for the evolution of the system from $t = 0$ to $t = \infty$ are given by

$$\frac{d[N_2]}{dt} = -k_{\text{off}}[N_2] + k_{\text{on}}[N]^2 \quad (10)$$

$$\frac{d[NS]}{dt} = -k_{\text{off}}[NS] + k_{\text{on}}[N][S] \quad (11)$$

combining eqs. 10 and 11 yields

$$\begin{aligned} \frac{d[N_2]}{dt} - \frac{d[NS]}{dt} &= -k_{\text{off}}[N_2] + k_{\text{off}}[NS] + k_{\text{on}}[N]^2 - k_{\text{on}}[N][S] \\ \frac{d[N_2]}{dt} - \frac{d(2c-2[N_2])}{dt} &= -k_{\text{off}}[N_2] + k_{\text{off}}[NS] + k_{\text{on}}[N]^2 - k_{\text{on}}[N][N] \\ \frac{d[N_2]}{dt} + 2\frac{d[N_2]}{dt} &= -k_{\text{off}}[N_2] + k_{\text{off}}(2c - 2[N_2]) \\ \frac{3d[N_2]}{dt} &= -k_{\text{off}}(3[N_2] - 2c) \\ \frac{3d[N_2]}{(3[N_2]-2c)} &= -k_{\text{off}}dt \\ \frac{d[N_2]}{[N_2]-\frac{2}{3}c} &= -k_{\text{off}}dt \end{aligned} \quad (12)$$

Integration yields

$$\begin{aligned} \int_c^{[N_2](t)} \frac{d[N_2]}{[N_2]-\frac{2}{3}c} &= -k_{\text{off}} \int_0^t dt \\ \ln\left([N_2](t) - \frac{2}{3}c\right) - \ln\left(c - \frac{2}{3}c\right) &= -k_{\text{off}}t \\ \ln\left(\frac{[N_2](t)-\frac{2}{3}c}{\frac{1}{3}c}\right) &= -k_{\text{off}}t \\ \frac{[N_2](t)-\frac{2}{3}c}{\frac{1}{3}c} &= \exp(-k_{\text{off}}t) \end{aligned} \quad (13)$$

With the final result

$$\begin{aligned} [N_2](t) &= \frac{1}{3}c \exp(-k_{\text{off}}t) + \frac{2}{3}c \\ [S_2](t) &= \frac{1}{3}c \exp(-k_{\text{off}}t) + \frac{2}{3}c \\ [NS](t) &= \frac{2}{3}c - \frac{2}{3}c \exp(-k_{\text{off}}t) \end{aligned} \quad (14)$$

Supplementary Figure 10 shows a numeric simulation of eqs. 14.

The observed NMR signal in the lifetime experiment is given by

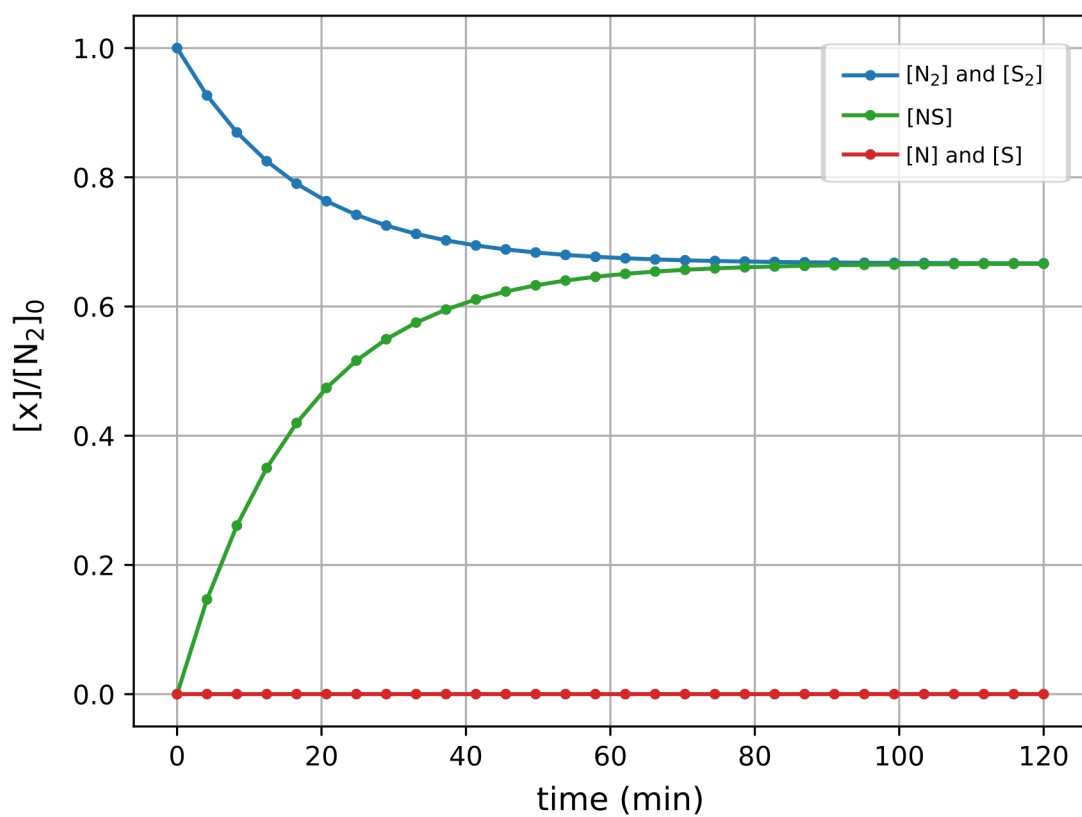
$$I(t) = a_1[N_2](t) + a_2[NS](t) = \left(\frac{1}{3}a_1 - \frac{2}{3}a_2\right) \cdot c \exp(-k_{\text{off}}t) + (a_1 + a_2) \frac{2}{3}c \quad (15)$$

where a_1 and a_2 are the specific molar NMR intensities of the N_2 and NS species, respectively. Since a_1 , a_2 and c are constants, eq. 15 can be rewritten as

$$I(t) = (I_0 - I_\infty) \cdot \exp(-k_{\text{off}}t) + I_\infty \quad (16)$$

where the constants I_0 and I_∞ are the signal intensities at $t = 0$ and $t = \infty$, respectively. The off-rate constant k_{off} can be obtained from non-linear fits of experimental data to eq. 16 or to the equivalent form

$$I_\Delta(t) = I(t) - I_\infty = (I_0 - I_\infty) \cdot \exp(-k_{\text{off}}t) \quad (17)$$



Supplementary Figure 10 | Numerical simulation integration of equations 11 and 12 with parameters $K_d = 2\mu\text{M}$, $k_{\text{off}} = 0.001\text{ s}^{-1}$, $[N]_{\text{total}} = 100\text{ }\mu\text{M}$.

Supplementary References

1. Hsu, S.T. & Dobson, C.M. ^1H , ^{15}N and ^{13}C assignments of the dimeric ribosome binding domain of Trigger Factor from *Escherichia coli*. *Biomol. NMR Assign.* **3**, 17–20 (2009).
2. Saio, T., Guan, X., Rossi, P., Economou, A. & Kalodimos, C.G. Structural basis for protein antiaggregation activity of the Trigger Factor chaperone. *Science* **344**, 1250494 (2014).
3. Benfield, C.T. *et al.* Mapping the I κ B kinase β (IKK β)-binding interface of the B14 protein, a vaccinia virus inhibitor of IKK β -mediated activation of nuclear factor κ B. *J. Biol. Chem.* **286**, 20727–20735 (2011).